Photogrammetric Modeling of Linear Features with Generalized Point Photogrammetry

Zuxun Zhang, Yongjun Zhang, Jianging Zhang, and Hongwei Zhang

Abstract

Most current digital photogrammetric workstations are based on feature points. Curved features are quite difficult to be modeled because they cannot be treated as feature points. The focus of the paper is on the photogrammetric modeling of space linear features. In general, lines and curves can be represented by a series of connected points, so called, generalized points in the paper. Different from all existing models, only one collinearity equation is used for each point on the linear curve, which makes the mathematical model very simple. Hereby, the key of generalized point photogrammetry is that all kinds of features are treated as generalized points to use either x or y collinearity equation. A significant difference between generalized point photogrammetry and conventional point photogrammetry is that image features are not necessarily exact conjugates. The exact conjugacy between image features and/or the correspondence between space and image feature are established during bundle block adjustment. Photogrammetric modeling of several space linear features is discussed. Sub-pixel precision has been achieved for both exterior orientation and 3D modeling of linear features, which verifies the correctness and effectiveness of the proposed approach.

Introduction

The collinearity equation among photographic center, space feature point, and the corresponding image point is the basic formulation of photogrammetry (Kraus, 1993; Mikhail and Bethel, 2001). It is called point photogrammetry (Guelch, 1995). Photogrammetric manipulation of imagery is a point-based operation. But points in photogrammetry mean only physical or visible points, such as dots, crosses, and corners. The main feature, which can be effectively measured, is a physical point in analogue, analytical, and digital photogrammetry.

Mulawa and Mikhail (1988) introduced the concept of linear feature and presented the formulation for photogrammetric observations and analytical linear features, such as straight lines and conics, in photogrammetric treatments. They chose to represent the 3D line by a point along the line and its direction vector. However, this representation is not unique. So, two constraints were applied: the norm of the direction vector was chosen as unity and the point along the line was chosen as the closest point to the origin.

There are many straight lines in architectural, archaeological, and industrial photogrammetry. If a space line is observed, the corresponding image line should lie in the plane determined by the photographic center and the space line, the so called coplanarity equation. The conventional point photogrammetry is not suitable for these applications. So interest in line photogrammetry based on the coplanarity equation and hybrid point-line photogrammetry based on both collinearity and coplanarity equations has greatly increased in the past years (Debevec, 1996; Baillard and Zisserman, 1999; Heuvel, 2003; Zhang *et al.* 2005).

High-level linear features, such as roads, rivers, and lakes in aerial photogrammetry, or line segments, circles and curves in architectural and industrial applications, are more useful for subsequent processes since they contain more information than feature points. Coordinate transformation techniques with linear features are discussed by Mikhail and Weerawong (1997). Geometric constraints among linear features, which are very important in photogrammetric treatments, are also analyzed.

The use of linear features is especially applicable in mapping and updating of constructed areas, since man-made objects include lots of linear curves. Also, natural objects like riverbank lines and coastlines as well as vegetation boarders offer a good possibility to apply feature-based approach (Heikkinen, 2002). In change detection and map updating with images, the correspondence between vector map and image features have to be determined for exterior orientation. Usually, ground control points and the corresponding image points are manually selected from the vector map and the image. Then, the image parameters can be determined by the space resection process. However, few apparent points can be identified in the map, which makes this solution less efficient in most cases. It is advantageous if the linear features can be used as control information.

Free-form linear features are used as control information in single photo resection by Habib *et al.* (2003a). One-to-one correspondence between image and object space primitives is not needed for the proposed approach since it is based on the modified iterated Hough transformation. Linear features are used for exterior orientation of linear-scanner satellite images with affine transformation model by Zhang *et al.* (2004). Although promising results have been achieved, the proposed model cannot deal with traditional aerial images.

Yongjun Zhang, Zuxun Zhang, and Jianqing Zhang are with the School of Remote Sensing and Information Engineering, Wuhan University, No. 129 Luoyu Road, Wuhan, 430079, P.R. China (zhangyj@whu.edu.cn).

Hongwei Zhang is with the National Geomatics Center of China, No.1 Baishengcun, Zizhuyuan, Beijing, 100044, P.R. China.

Photogrammetric Engineering & Remote Sensing
Vol. 74, No. 9, September 2008, pp. 1119–1127.

0099-1112/08/7409–1119/$3.00/0

Straight lines and linear features are successfully used as control information in aerial triangulation by Schenk (2004) and Akav *et al.* (2004), respectively.

However, the reconstruction of space linear features is still in an early stage, because they cannot be effectively measured by current digital photogrammetric workstations. Dey and Wenger (2001) proposed a technique to reconstruct a planar curve by sharp corners. In spite of its good performance, the theoretical guarantee of the algorithm could not be proved (Dey and Wenger, 2001). An automatic relative orientation approach with linear features is presented by Habib and Kelley (2001); then, the points on the 3D curve are determined by forward intersection with conjugate image points (Habib *et al.*, 2003b). The problem is the difficulty to identify conjugate points along the curve. Thus, pruning techniques are used to resolve the ambiguities.

The model of generalized point photogrammetry is discussed in the next section. Then models of several linear features with generalized point photogrammetry are presented. Afterwards, experiments of exterior orientation by matching between vector and image, reconstruction of circles and rounded rectangles, and 3D modeling of space curves are presented. Finally, conclusions are briefly outlined.

Model of Generalized Point Photogrammetry

In conventional point photogrammetry, collinearity equations are used for physical points (Mikhail and Bethel, 2001):

$$x = x_0 - f\frac{a_1(X - X_S) + b_1(Y - Y_S) + c_1(Z - Z_S)}{a_3(X - X_S) + b_3(Y - Y_S) + c_3(Z - Z_S)} \quad (1)$$

$$y = y_0 - f\frac{a_2(X - X_S) + b_2(Y - Y_S) + c_2(Z - Z_S)}{a_3(X - X_S) + b_3(Y - Y_S) + c_3(Z - Z_S)} \quad (2)$$

where x and y are the observations, X, Y, and Z the coordinates of ground point, a_i, b_i, c_i ($i = 1, 2, 3$) the orientation matrix composed of rotation angles φ, ω, and κ where the Y-axis is taken as the primary axis, and X_S, Y_S, Z_S, φ, ω, κ, f, x_0, y_0 are the exterior and interior parameters. If $p_1, \ldots, p_n$ are additional parameters incorporated into the collinearity equations, the linearized observation equations can be written as:

$$\begin{aligned} v_x = {} & a_{11}\Delta X_s + a_{12}\Delta Y_s + a_{13}\Delta Z_s + a_{14}\Delta\varphi + a_{15}\Delta\omega + a_{16}\Delta\kappa \\ & + a_{17}\Delta f + a_{18}\Delta x_0 + a_{19}\Delta y_0 + b_{11}\Delta X + b_{12}\Delta Y + b_{13}\Delta Z \\ & + c_{11}\Delta p_1 + \cdots + c_{1n}\Delta p_n - l_x \end{aligned} \quad (3)$$

$$\begin{aligned} v_y = {} & a_{21}\Delta X_s + a_{22}\Delta Y_s + a_{23}\Delta Z_s + a_{24}\Delta\varphi + a_{25}\Delta\omega + a_{26}\Delta\kappa \\ & + a_{27}\Delta f + a_{28}\Delta x_0 + a_{29}\Delta y_0 + b_{21}\Delta X + b_{22}\Delta Y + b_{23}\Delta Z \\ & + c_{21}\Delta p_1 + \cdots + c_{2n}\Delta p_n - l_y \end{aligned} \quad (4)$$

where v_x, v_y are the corrections of observations, ΔX, ΔY, ΔZ the corrections of ground point, ΔX_S, ΔY_S, ΔZ_S, $\Delta\varphi$, $\Delta\omega$, $\Delta\kappa$, and Δf, Δx_0, Δy_0 are the corrections of exterior and interior parameters. Coefficients of unknowns are:

$$a_{11} = \frac{\partial x}{\partial X_S},\ a_{12} = \frac{\partial x}{\partial Y_S},\ a_{13} = \frac{\partial x}{\partial Z_S},\ a_{14} = \frac{\partial x}{\partial \varphi},$$

$$a_{15} = \frac{\partial x}{\partial \omega},\ a_{16} = \frac{\partial x}{\partial \kappa}$$

$$a_{21} = \frac{\partial y}{\partial X_S},\ a_{22} = \frac{\partial y}{\partial Y_S},\ a_{23} = \frac{\partial y}{\partial Z_S},\ a_{24} = \frac{\partial y}{\partial \varphi},$$

$$a_{25} = \frac{\partial y}{\partial \omega},\ a_{26} = \frac{\partial y}{\partial \kappa}$$

$$a_{17} = \frac{\partial x}{\partial f},\ a_{18} = \frac{\partial x}{\partial x_0},\ a_{19} = \frac{\partial x}{\partial y_0}$$

$$a_{27} = \frac{\partial y}{\partial f},\ a_{28} = \frac{\partial y}{\partial x_0},\ a_{29} = \frac{\partial y}{\partial y_0}$$

$$b_{11} = \frac{\partial x}{\partial X},\ b_{12} = \frac{\partial x}{\partial Y},\ b_{13} = \frac{\partial x}{\partial Z},\ b_{21} = \frac{\partial y}{\partial X},$$

$$b_{22} = \frac{\partial y}{\partial Y},\ b_{23} = \frac{\partial y}{\partial Z}$$

$$c_{11} = \frac{\partial x}{\partial p_1}, \ldots\ldots\ldots, c_{1n} = \frac{\partial x}{\partial p_n},$$

$$c_{21} = \frac{\partial y}{\partial p_1}, \ldots\ldots\ldots, c_{2n} = \frac{\partial y}{\partial p_n}$$

where $l_x = x - (x)$ and $l_y = y - (y)$, where (x) and (y) are computed from Equations 1 and 2 with approximate camera parameters and coordinates of ground features.

If the above collinearity equations are used to determine 3D objects, conjugate image points have to be identified. All the current digital photogrammetric workstations are based on the collinearity equations. However, matching between point features is more difficult than matching between linear features. Debevec (1996) proposed a hybrid geometry- and image-based approach to reconstruct architectures. As shown in Figure 1a, error between the observed image edge $\{(x_1, y_1), (x_2, y_2)\}$ and the predicted image line is defined as the shortest distance *hs* from a point *p(s)* on the segment to the predicted line (Debevec, 1996). This definition leads to an integral error function, which is difficult to be incorporated into the collinearity equations.

Same as that of Debevec (1996), most current methods deal with linear features by minimizing the distance between a point and a linear feature. However, the mathematical model is very complicated and difficult to be used for mass data block adjustment. Moreover, 3D reconstruction of curved features seems more difficult with this strategy. The situation would be much better if the distance defined above is divided into two components along the x-axis and y-axis of the image coordinate system. The disparity between the predicted and observed line can be calculated in a simple way. dx_1 (dy_1) and dx_2 (dy_2) represent the difference from the two end points of the image edge to the predicted line along the x-axis (y-axis), as shown in Figure 1a and 1b, respectively. Instead of using h_1 and h_2 as the error function, dx_1 and dx_2 or dy_1 and dy_2 are used if the slope of the observed edge is larger than 1.0 (the angle of inclination α of a edge is in the range $45° \le \alpha \le 135°$ or $225° \le \alpha \le 315°$) or smaller than 1.0 (the angle of inclination α of a edge is in the range $135° \le \alpha \le 225°$ or $-45° \le \alpha \le 45°$), respectively, because the vertical shift dy or horizontal shift dx of the edge has a limited contribution to minimize the disparity between the predicted and observed line. This is the basic conception of generalized point photogrammetry.

Different from all existing models, only one equation is used for each observed generalized point in our model. Note that in the above definition of error function, the biggest advantage is that the exact conjugacy between image features and/or the exact correspondence between space and image feature is not a prerequisite for generalized point. Moreover, space lines and curves can be expressed by a series of connected points. Hereby, the key of generalized point photogrammetry is that all kinds of features are treated as generalized points and incorporated into extended collinearity equations.

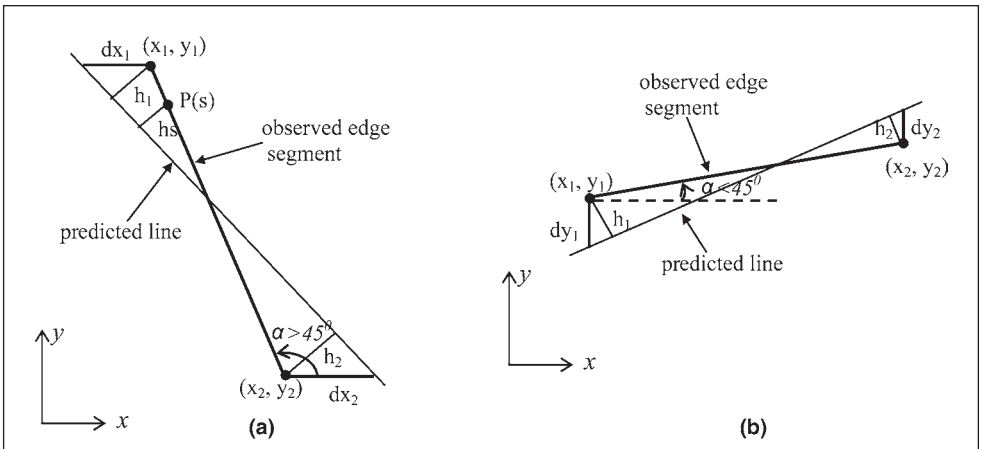

Figure 1. Model of generalized point photogrammetry: the error between the (a) observed image edge, and (b) the predicted image line.

The most significant difference between generalized point and physical point is that image features are not necessarily conjugate ones for generalized point. Another difference is that in the two collinearity equations x and y are used for a physical point, while only one collinearity equation x or y is used for a generalized point. Moreover, the collinearity equation used by generalized point includes the parameters of the space feature, for example the coordinates of generalized point is expressed by parameters of space features. When incorporated into the collinearity equation, parameters of the interested object can be obtained by bundle adjustment.

Modeling Linear Features with Generalized Point Photogrammetry

In generalized point photogrammetry, parameters of space features are incorporated into the collinearity equations. The conjugacy between image features and/or the correspondence between space and image feature are established during the bundle block adjustment. The model of generalized point photogrammetry for several kinds of linear features, such as space circle, straight line, and curve will be discussed in the following.

Circle

Six parameters, i.e., the center (X_0, Y_0, Z_0), the orientation (β, γ, 0) and the radius R, are enough to determine a space circle because the third rotation angle is of no influence and thus treated as zero. In this case, the orientation matrix of the plane where a circle lies in is:

$$R' = \begin{pmatrix} \cos\beta & -\sin\beta\sin\gamma & -\sin\beta\cos\gamma \\ 0 & \cos\gamma & -\sin\gamma \\ \sin\beta & \cos\beta\sin\gamma & \cos\beta\cos\gamma \end{pmatrix} \quad (5)$$

so that any point on the space circle can be represented as:

$$\begin{cases} X = R(\cos\beta\cos\theta - \sin\beta\sin\gamma\sin\theta) + X_0 \\ Y = R(\cos\gamma\sin\theta + Y_0 \\ Z = R(\sin\beta\cos\theta + \cos\beta\sin\gamma\sin\theta) + Z_0 \end{cases} \quad (6)$$

where X_0, Y_0, Z_0 the circle center, β and γ the orientation angles of the plane in which the circle lies, and R the radius. θ varies from 0 to 360 degrees for a circle, or from specific start to end angle for and arc. Incorporating Equation 6 into collinearity Equations 1 and 2 leads to:

$$x = x_0 - f\frac{\begin{array}{l} a_1(X_0 + R(\cos\beta\cos\theta - \sin\beta\sin\gamma\sin\theta) \\ \quad - X_S) + b_1(Y_0 + R(\cos\gamma\sin\theta) - Y_S) + c_1(Z_0 \\ \quad + R(\sin\beta\cos\theta + \cos\beta\sin\gamma\sin\theta) - Z_S) \end{array}}{\begin{array}{l} a_3(X_0 + R(\cos\beta\cos\theta - \sin\beta\sin\gamma\sin\theta) \\ \quad - X_S) + b_3(Y_0 + R(\cos\gamma\sin\theta) - Y_S) + c_3(Z_0 \\ \quad + R(\sin\beta\cos\theta + \cos\beta\sin\gamma\sin\theta) - Z_S) \end{array}} \quad (7)$$

$$y = y_0 - f\frac{\begin{array}{l} a_2(X_0 + R(\cos\beta\cos\theta - \sin\beta\sin\gamma\sin\theta) \\ \quad - X_S) + b_2(Y_0 + R(\cos\gamma\sin\theta) - Y_S) + c_2(Z_0 \\ \quad + R(\sin\beta\cos\theta + \cos\beta\sin\gamma\sin\theta) - Z_S) \end{array}}{\begin{array}{l} a_3(X_0 + R(\cos\beta\cos\theta - \sin\beta\sin\gamma\sin\theta) \\ \quad - X_S) + b_3(Y_0 + R(\cos\gamma\sin\theta) - Y_S) + c_3(Z_0 \\ \quad + R(\sin\beta\cos\theta + \cos\beta\sin\gamma\sin\theta) - Z_S) \end{array}}. \quad (8)$$

The parameters in the above equations can be divided into exterior orientation parameters and object related parameters. In this case, the additional parameters are $p_1 = X_0$, $p_2 = Y_0$, $p_3 = Z_0$, $p_4 = \beta$, $p_5 = \gamma$, and $p_6 = R$. The coefficients of exterior orientation parameters are the same as that of Equations 3 and 4. The coefficients of object related parameters could be obtained by partial derivatives in a similar way.

As shown in Figure 2a, a generalized point A is computed from the circle parameter at angle θ. The tangential vector (with angle α) of the received image point a can be determined. Equation 7 is used for exterior orientation or 3D reconstruction if $45° \le \alpha \le 135°$ or $225° \le \alpha \le 315°$; otherwise Equation 8 is used.

Principally, two images are enough to reconstruct a space circle, as shown in Figure 2b. Image points a_1, a_1' and a_2, a_2' are conjugate points of the stereo. Points A_1 and A_2 on the space circle can be easily determined by forward intersection. However, to ensure the stability and accuracy of reconstruction, three or more overlapping images are expected. If a circle is used for exterior orientation, the unknowns of circle parameters are to be eliminated from the observation equations.

Straight Line

If the plane where a space line lies in is unknown, several parameters have to be introduced to represent the line.

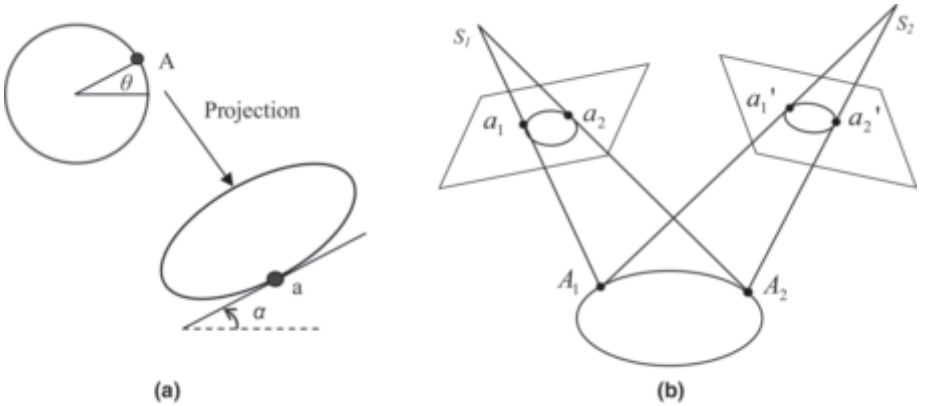

Figure 2. Circle reconstruction with generalized point photogrammetry: (a) a generalized point *A* computed from the circle parameter, and (b) reconstruction of a space circle from two images.

Although four independent parameters are enough to uniquely present a space line segment *L*, six parameters are used for the convenience of incorporating into collinearity equations:

$$\begin{cases} X = X_0 + t \cdot \cos\beta \\ Y = Y_0 + t \cdot \cos\gamma \quad (a \le t \le b) \\ Z = Z_0 + t \cdot \cos\kappa \end{cases} \tag{9}$$

where (X_0, Y_0, Z_0) is the start point, (β, γ, κ) the direction angle of the line, t the distance from a certain point on the line to the start point, and a and b the range of parameter t.

Incorporating Equation 9 into collinearity Equations 1 and 2 leads to:

$$x = x_0 - f\frac{a_1(X_0 + t\cos\beta - X_S) + b_1(Y_0 + t\cos\gamma - Y_S) + c_1(Z_0 + t\cos\kappa - Z_S)}{a_3(X_0 + t\cos\beta - X_S) + b_3(Y_0 + t\cos\gamma - Y_S) + c_3(Z_0 + t\cos\kappa - Z_S)} \tag{10}$$

$$y = y_0 - f\frac{a_2(X_0 + t\cos\beta - X_S) + b_2(Y_0 + t\cos\gamma - Y_S) + c_2(Z_0 + t\cos\kappa - Z_S)}{a_3(X_0 + t\cos\beta - X_S) + b_3(Y_0 + t\cos\gamma - Y_S) + c_3(Z_0 + t\cos\kappa - Z_S)}. \tag{11}$$

The coefficients of exterior orientation parameters in Equations 10 and 11 are the same as that of Equations 3 and 4. The coefficients of object related parameters could be obtained by partial derivatives in a similar way. One of the two collinearity equations can be applied to each end point of a straight line. As shown in Figure 3a, if the angle α (defined by the direction of an image line against *x*-axis) of the observed line *l* is in the range $45° \le \alpha \le 135°$ or $225° \le \alpha \le 315°$, Equation 10 is used taken dx_1 and dx_2 as the error function, which represent the difference from the two end points of the image edge to the predicted line along the *x*-axis. Otherwise, Equation 11 is used taken dy_1 and dy_2 as the error function, which represent the difference from the two end points of the image edge to the predicted line along the *y*-axis, as shown in Figure 3b. Note that any point on the line except the two end points has no contribution on minimizing the disparity. So, one image line can afford two observation equations. All the six parameters should be unknowns to determine a space line segment with at least two stereo images. Caution must be exercised to avoid viewing the straight line solely as an epipolar view. For example, suppose that two images of an interested space line fall into an epipolar line between two perspective centers; then, the line cannot be determined.

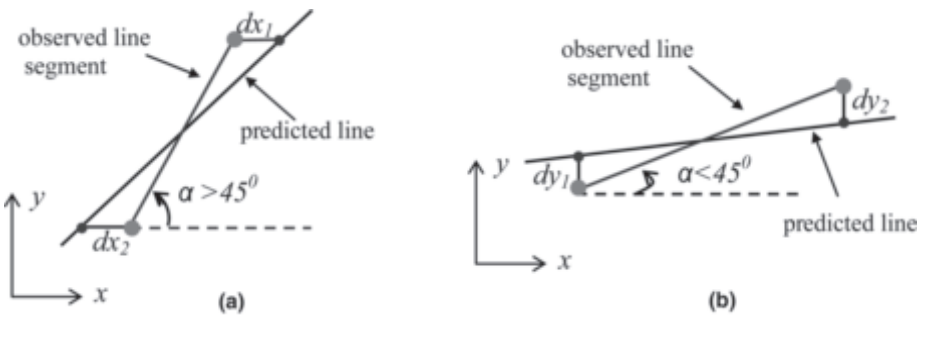

Figure 3. Line reconstruction with generalized point photogrammetry representing the difference from the two end points of the image edge to the predicted line along (a) the *x*-axis (Equation 10), and (b) the *y*-axis (Equation 11).

If space lines are used for exterior orientation, the line-related unknowns should be eliminated from the observation equations. In this case, the space resection process only requires a minimum of three straight lines. However, the degenerate cases must be avoided. For example, three parallel lines or three lines that intersect at a common point will not give a unique solution.

Curve

Usually, a space curve can be parameterized as:

$$\begin{cases} X = f(t) \\ Y = g(t) \quad (a \le t \le b) \\ Z = h(t) \end{cases} \tag{12}$$

where $f(t)$, $g(t)$, and $h(t)$ the locus of points on the space curve as a function of curve parameter t, ranging from a to b. Incorporating Equation 12 into Equations 1 and 2 leads to:

$$x = x_0 - f\frac{a_1(f(t) - X_S) + b_1(g(t) - Y_S) + c_1(h(t) - Z_S)}{a_3(f(t) - X_S) + b_3(g(t) - Y_S) + c_3(h(t) - Z_S)} \tag{13}$$

$$y = y_0 - f\frac{a_2(f(t) - X_S) + b_2(g(t) - Y_S) + c_2(h(t) - Z_S)}{a_3(f(t) - X_S) + b_3(g(t) - Y_S) + c_3(h(t) - Z_S)}. \tag{14}$$

Suppose the tangential vector of a point on the observed image curve is α (as shown in Figure 4), Equation 13 is used for exterior orientation and 3D reconstruction if $45° \le \alpha \le 135°$ or $225° \le \alpha \le 315°$, otherwise Equation 14 is used. The above model can be used for exterior orientation, reconstruction of space curves, or both of them in a bundle block adjustment.

For exterior orientation, the space curves need not to be analytical ones. They could be arbitrary free form linear features as long as they can be represented by a series of connected points. The disparity between the observed image feature and the projected space feature is smaller and smaller during iterations, an artist impression is shown in Figure 4a, 4b, 4c, and 4d, respectively. The disparity usually converges within several iterations. If a space curve is photographed in at least two stereo images, the image parameters and the model of the curve may be solved by an iterative bundle adjustment with Equations 13 and 14 simultaneously. To ensure the stability of adjustment, more than two overlapping images are expected. However, one should be careful that the parameter a and b in Equation 12 have to be known for opening curves, while it is not necessary to be known for closed curves, such as circles and ellipses. Degenerate cases must be avoided to reconstruct the linear curves. For example, the perspective center falls in the plane where a 3D planar curve lies. In this case, the image feature will be an edge instead of a curved linear feature.

Experiments of Modeling Linear Features

From the principle described above, it is easy to combine physical points, straight lines, circles, and linear curves into one adjustment model. This model is possible for reconstruction of space features that can be represented by mathematical models. The advantage of using linear features is that one is more likely to find geometric constraints among linear features than among point features. In order to stabilize the adjustment procedure, geometric constraints among selected object features, such as perpendicular features, parallel lines, same end points, coplanar features, etc., should be added into the bundle adjustment to solve the parameters of multiple features simultaneously.

Exterior Orientation with Linear Features

One of the key procedures in map updating is how to fully utilize the information extracted from vector map to determine the image orientation parameters. However, few apparent points can be identified in the map, which makes the map updating process less efficient. Therefore, instead of selecting control points manually, taking widely existing free-form linear features as control information is very important to improve both efficiency and accuracy. Different from Zhang *et al.* (2004) that concentrate on linear-scanner

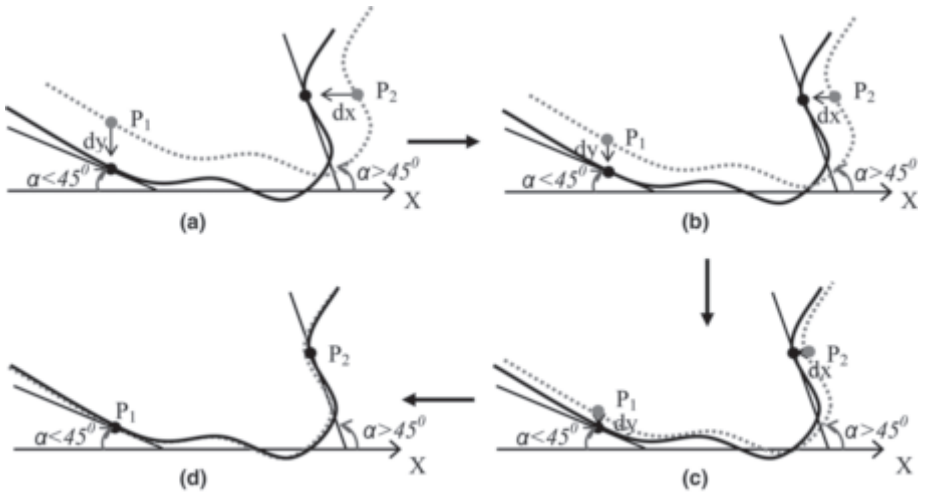

Figure 4. Iterative curve reconstruction with generalized point photogrammetry. An artistic impression of the disparity between the observed image feature and the projected space feature becoming smaller and smaller in (a), (b), (c), and (d), respectively. A color version of this figure is available at the ASPRS website: **www.asprs.org**.

satellite images, traditional aerial frame images are considered in this paper. Usually, three control points is enough to establish coarse correspondence between the image and space linear features, then image parameters can be determined by minimizing the disparity between the image and space linear features with the previously described model.

In the test area, aerial frame images are taken at a scale 1:15 000 and scanned with 0.025 mm pixel size. The scale of vector data is 1:10 000, i.e., the precision of vector data is a little bit higher than 2 meters. The point in Figure 5 is one of three manually-measured control points (about five pixel accuracy) to determine the initial image parameters. The linear features are the projected space features with the image parameters determined by the three control points. In this step, the corresponding image features are usually more than 20 pixels away from the projected space features. It is easy to imagine that the farther the distance from control points, the larger the disparity between image and projected space feature. However, it is enough to represent the initial correspondence between space and image features. A representative region is highlighted by bold rectangle, and separately shown in Figure 6. The linear features around the road center are the extracted image features. Although five times zoomed out, there are significant disparities between the image and projected space features because image parameters obtained from the three control points are not accurate enough. Figure 7 shows the final projections of linear features after exterior orientation with the control linear features. Precision of exterior orientation with linear features is about 1.0 pixel. It is clear that the vector data is well fitted to the image features.

After determining the parameters of a stereo pair by the above strategy, ground checkpoints measured from the vector map are used to evaluate the precision of exterior orientation. The image points corresponding to each checkpoint are manually measured. Then, the 3D coordinates of each checkpoint are computed by forward intersection with the above determined image parameters. Afterwards, the 3D coordinates are compared with the ground truth. The root mean square error of checkpoints is listed in Table 1. As can be seen, the error statistics of checkpoints is comparable with the precision of vector map. Moreover, the error statistics of the image pair with the checkpoints shown in Table 2 indicate that the RMSE of residues of image points also lays on pixel level, which shows that the proposed approach is feasible for exterior orientation with control linear features.

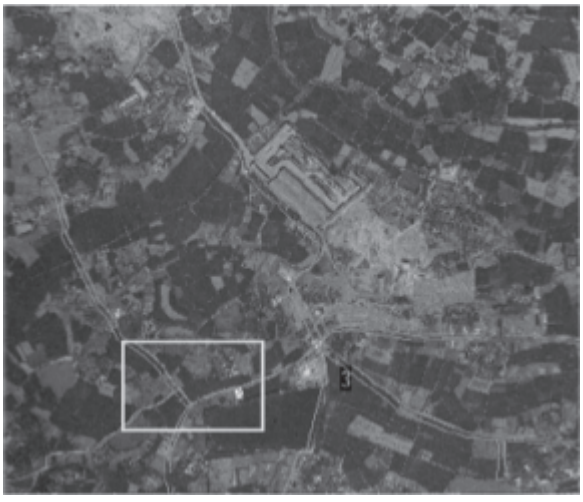

Figure 5. Initial projection of space linear features and the subject area. A color version of this figure is available at the ASPRS website: **www.asprs.org**.

Figure 6. Initial correspondence between space and image linear features of the subject area.

Figure 7. Projections of space linear features after exterior orientation. A color version of this figure is available at the ASPRS website: **www.asprs.org**.

Reconstruction of Circles and Rounded Rectangles

Automatic inspection of complex shapes such as circles and rounded rectangles on industrial parts is quite important for quality control. The proposed model of generalized point photogrammetry is successfully applied to reconstruct circles and rounded rectangles. The inspection platform is composed of a rotating table and a pre-calibrated CCD camera (see Zhang *et al.*, 2006 for more detail). The part to be inspected is put on the center of the table. Images are taken while the table rotating against its axis under computer

TABLE 1. ERROR STATISTICS OF EXTERIOR ORIENTATION WITH CONTROL LINEAR FEATURES (METERS)

Components	*X*	*Y*	*Z*
RMSE	1.63	1.36	1.87

TABLE 2. ERROR STATISTICS OF IMAGE CHECK POINTS (PIXELS)

		RMSE	1.02
	x	Max	1.63
Left		Min	−0.06
Image		RMSE	0.54
	y	Max	0.90
		Min	0.09
		RMSE	0.92
	x	Max	−1.72
Right		Min	0.16
Image		RMSE	0.84
	y	Max	1.32
		Min	0.22

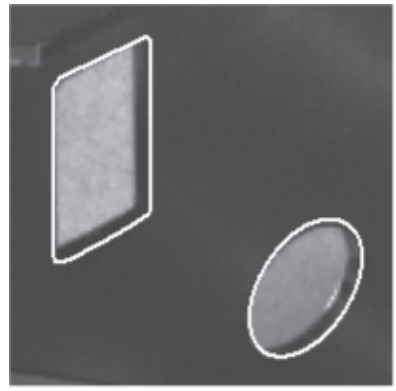

Figure 9. Projection of circle and rounded rectangle.

control. Based on generalized point photogrammetry, not only straight lines but also circles and rounded rectangles can be reconstructed accurately. The reconstruction process is subdivided into two steps. First, the wire-frame model of the industrial part and the corresponding image parameters are obtained by a bundle block adjustment. Afterwards, the circles and rounded rectangles are reconstructed according to the obtained image orientation parameters. Several constraints, such as coplanarity, perpendicularity, and connectivity are added in the bundle adjustment. One image of a sheetmetal part is shown in Figure 8. Since the purpose of this paper is to deal with complex shapes, the wire-frame model of the part is reconstructed with the model of hybrid point-line bundle adjustment. Image orientation parameters are also treated as known. The subject circle and rounded rectangle are highlighted with rectangle in Figure 8 and separately shown in Figure 9. Different from (Zhang *et al.*, 2006) that uses both *x* and *y* direction error equations, only one equation (either *x* or *y* as described in the previous section) is used to reconstruct circles and rounded rectangles, After reconstructed by the proposed model, projections of the circle and rounded rectangle are shown in Figure 9. Although such entities are very small, the reconstructed models are well fitted to the image features. Accuracy of reconstruction is comparable with that of (Zhang *et al.*, 2006), which verifies the correctness of the proposed model. Nevertheless, the mathematical model proposed in this paper is simpler than that of Zhang (Zhang *et al.*, 2006).

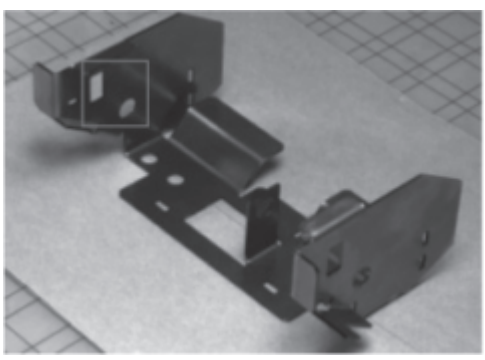

Figure 8. Measurable 3D geometric model.

Reconstruction of Curving Buildings

3D reconstruction and texture mapping of buildings are the main contents of 3D city modeling. Reconstruction of wire-frame building models that composed of straight-line segments with coarse-to-fine strategy is presented by Zhang *et al.* (2005). Complex buildings are also very important for city modeling. However, it is not possible to reconstruct complex (such as curving) buildings with the model proposed by Zhang *et al.* (2005) because only straight lines and feature points can be processed. Nevertheless, the model of generalized point photogrammetry proposed in this paper is capable of reconstructing these kinds of objects. The general strategy is the same as that of Zhang *et al.* (2005), which includes aerial triangulation, initial model generation, and coarse-to-fine modeling. The most important improvement is that modeling of generalized point photogrammetry is used to deal with complex shapes. The same data source as that of Zhang *et al.* (2005) is used for experiments in this paper. The ground resolution of stereo images is about 0.2 m. The precision of aerial triangulation is about 0.3 pixels, i.e., 0.06 m. To facilitate the process of 3D reconstruction, image parameters are treated as known since they are obtained from aerial triangulation. In this paper, complex buildings are presented by mathematical curves together with wire-frame model. Seven adjacent images are used to reconstruct this complex building. Figure 10 shows four image blocks of four adjacent images which contain the interested curving building. As shown in Figure 10, the curving part of the roof is flat, and thus it is assumed that all points on the curving feature have the same height $Z = Z_0$, so the curving feature of the roof is modeled as a cubic curve $Y - Y_0 = a_1(X - X_0) + a_2(X - X_0)^2 + a_3(X - X_0)^3$, where (X_0, Y_0, Z_0) is the starting point of the curve and also the end point of another line segment. Then, the 3D building model can be obtained from stereo pairs. In order to stabilize the adjustment procedure, constraints of perpendicular, parallel, coplanar, horizontal, and vertical among line segments and curves are added to solve the parameters simultaneously. Furthermore, the end points of cubic curves are also start points of roof edges. These constraints are vital to reconstruct the whole model uniquely. As

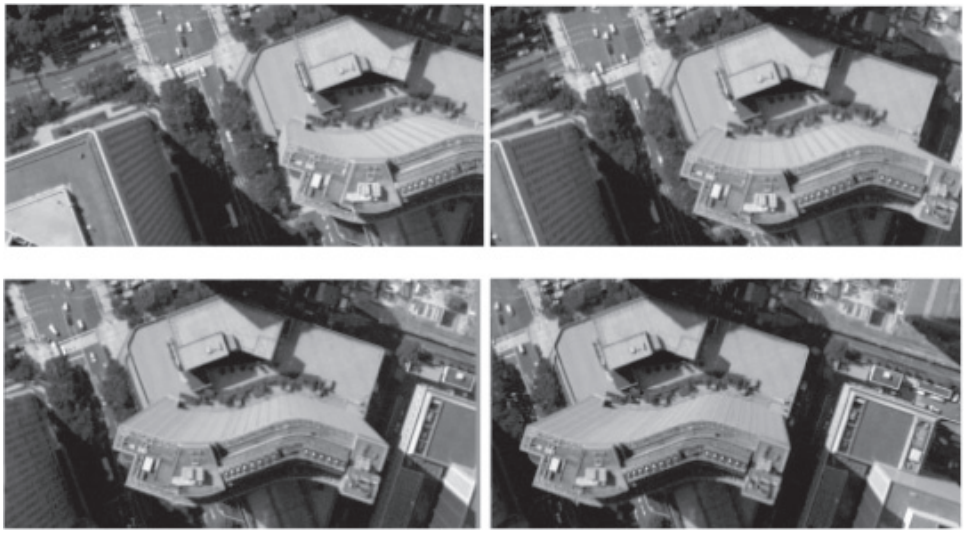

Figure 10. Four image blocks containing the subject curving building.

shown in Figure 11, the white lines and linear curves, which are projected with the reconstructed model, are well fitted to the image features. The accuracy of reconstructed building is about 0.15 m, slightly higher value than the image resolution.

Conclusions

The model of generalized point photogrammetry is proposed in this paper. The proposed approach can incorporate physical feature points, straight lines, circles, and linear curves into one mathematical model. The advantage of using linear features is that one is more likely to find geometric constraints among linear features than among point features. The biggest difference between generalized point photogrammetry and conventional point photogrammetry is that image features are not necessarily conjugate ones in generalized point photogrammetry. The exact conjugacy between image features and/or the correspondence between space and image feature are established during bundle block adjustment.

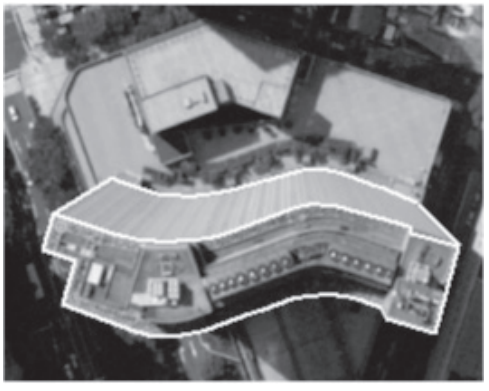

Figure 11. Reconstructed model of the subject curving building.

The proposed approach is capable of modeling space features that can be represented by analytical mathematical models. While for the space resection process, the control features can be any free-form linear features. The parameters of aerial stereo images are successfully obtained with free-form control linear features. Sub-pixel precision is achieved when handling complex buildings.

However, much attention should be paid to the modeling of linear features. If space lines are used for exterior orientation, the space resection process only requires a minimum of three straight lines, but, the degenerate cases must be avoided. For example, three parallel lines or three lines that intersect at a common point will not give a unique solution. Degenerate cases must also be avoided to reconstruct linear curves. For example, the perspective center falls in the plane where a 3D planar curve lies. In this case, the image feature will be an edge instead of a curved linear feature.

To ensure the stability of adjustment, more than two non-degenerate stereo images are required. Furthermore, geometric constraints among selected object features, such as perpendicular features, parallel lines, same end points, coplanar features, etc., should be added into the bundle adjustment. Otherwise, the result is unstable or even impossible to solve for the parameters of space features.

Acknowledgments

This work is supported by the State Key Basic Research and Development Program with Project No. 2006CB701302, National Natural Science Foundation of China (NSFC) with Project No. 40671157, 40301041, and 40337055. Heartfelt thanks are given for the comments and contributions of anonymous reviewers and members of the editorial team.

References

Akav, A., G.H. Zalmanson, and Y. Doytsher, 2004. Linear feature based aerial triangulation, *Proceedings of the International Archives of the Photogrammetry, Remote Sensing and Spatial*

Information Sciences, 12–23 July, Istanbul, Turkey, 35 (B/3):7–12.

Baillard, C., and A. Zisserman, 1999. Automatic reconstruction of piecewise planar models from multiple views, *Proceedings of the IEEE Conference on Computer Vision and Pattern Recognition*, 23–25 June, Fort Collins, Colorado, pp. 559–565.

Debevec, P.E., 1996. *Modeling and Rendering Architecture from Photographs*, Ph.D. thesis, University of California at Berkeley, 140 p.

Dey, T.K., and R. Wenger, 2001. Reconstructing curves with sharp corners, *Computational Geometry Theory & Applications*, 19(2–3):89–99.

Guelch, E., 1995. Line photogrammetry: A tool for precise localization of 3D points and lines in automated object reconstruction, *Proceedings of SPIE – Integrating Photogrammetric Techniques with Scene Analysis and Machine Vision II*, April 19–21, Orlando, Florida, 2486:2–12.

Habib, A., and D. Kelley, 2001. Automatic relative orientation of large scale imagery over urban areas using modified iterated Hough transform, *Journal of Photogrammetry and Remote Sensing*, 56(1):29–41.

Habib, A., H.T. Lin, and M. Morgan, 2003a. Autonomous space resection using point- and line-based representation of free-form control linear features, *The Photogrammetric Record*, 18(103):244–258.

Habib, A., Y. Lee, and M. Morgan, 2003b. Automatic matching and three-dimensional reconstruction of free-form linear features from stereo images, *Photogrammetric Engineering & Remote Sensing*, 69(2):189–197.

Heikkinen, J., 2002. Feature Based Photogrammetry, Helsinki University of Technology, Finland, URL: http://foto.hut.fi/opetus/290/julkaisut/Jussi_Heikkinen/FeatureBasedPhoto.pdf (last date accessed: 13 May 2008).

Heuvel, F.A. van den, 2003. *Automation in Architectural Photogrammetry, Line Photogrammetry for the Reconstruction from Single and Multiple Images*, Ph.D. thesis, Technical University of Delft, 190 p.

Kraus, K., 1993. *Photogrammetry, Volume 1, Fundamentals and Standard Processes*, Dummler Verlag, Bonn, 389 p.

Mikhail, E.M., and K. Weerawong, 1997. Exploitation of linear features in surveying and photogrammetry, *Journal of Surveying Engineering*, 123(1):32–47.

Mikhail, E.M., and J.S. Bethel, 2001. *Introduction to Modern Photogrammetry*, John Wiley & Sons, Inc., 496 p.

Mulawa, D.C., and E.M. Mikhail, 1988. Photogrammetric treatment of linear features, *Proceedings of the International Archives of Photogrammetry, Remote Sensing and Spatial Information Sciences*, 01–10 July, Kyoto, Japan, Commission III, 27(B10): 383–393.

Schenk, T., 2004. From point-based to feature-based aerial triangulation, *Journal of Photogrammetry and Remote Sensing*, 58:315–329.

Zhang, J., H. Zhang, and Z. Zhang, 2004. Exterior orientation for remote sensing image with high resolution by linear feature, *Proceedings of The International Archives of the Photogrammetry, Remote Sensing and Spatial Information Sciences*, 12–23 July, Istanbul, Turkey, 35(B/3):76–79.

Zhang, Y., Z. Zhang, J. Zhang, and J. Wu, 2005. 3D building modelling with digital map, LIDAR data and video image sequences, *The Photogrammetric Record*, 20(111):285–302.

Zhang, Y., Z. Zhang, and J. Zhang, 2006. Automatic measurement of industrial sheetmetal parts with CAD data and non-metric image sequence, *Computer Vision and Image Understanding*, 102:52–59.

Zhang, Z., and J. Zhang, 2004. Generalized point photogrammetry and its application, *Proceedings of The International Archives of the Photogrammetry, Remote Sensing and Spatial Information Sciences*, 12–23 July, Istanbul, Turkey, 35(B/5):77–81.

(Received 17 May 2006; accepted 10 July 2006; revised 15 November 2006)